Inorg. Chem. **2003**, *42*, 8353–8365

Phosphate Diester Hydrolysis and DNA Damage Promoted by New *cis*-Aqua/Hydroxy Copper(II) Complexes Containing Tridentate Imidazole-rich Ligands

Marciela Scarpellini,[†] Ademir Neves,*[,†] Rosmari Hörner,[†] Adailton J. Bortoluzzi,[†] Bruno Szpoganics,[†] César Zucco,[†] René A. Nome Silva,[†] Valderes Drago,[‡] Antônio S. Mangrich,[§] Wilson A. Ortiz,[||] Wagner A. C. Passos,[||] Maurício C. B. de Oliveira,[⊥] and Hernán Terenzi[⊥]

Laboratório de Bioinorgânica e Cristalografia, Departamento de Química, Universidade Federal de Santa Catarina, 88040-900, Florianópolis, SC, Brazil, Departamento de Física, Universidade Federal de Santa Catarina, 88040-900, Florianópolis, SC, Brazil, Departamento de Química, Universidade Federal do Paraná, 81531-970, Curitiba, PR, Brazil, Grupo de Supercondutividade e Magnetismo, Universidade Federal de São Carlos, 13565-900, São Carlos, SP, Brazil, and Laboratório de Expressão Gênica, Departamento de Bioquímica, Universidade Federal de Santa Catarina, 88040-900, Florianópolis, SC, Brazil

Received December 17, 2002

The tridentate Schiff base [(2-(imidazol-4-yl)ethyl)(1-methylimidazol-2-yl)methyl)imine (HISMIMI) and its reduced form HISMIMA were synthesized and characterized, as well their mononuclear *cis*-dihalo copper(II) complexes **1** and **2**, respectively. In addition, the dinuclear $[Cu^{II}(\mu\text{-}OH)_2Cu^{II}]^{2+}$ complexes (**3**) and (**4**) obtained from complexes **1** and **2**, respectively, were also isolated and characterized by several physicochemical techniques, including magnetochemistry, electrochemistry, and EPR and UV–vis spectroscopies. The crystal structures of **1** and **2** were determined by X-ray crystallography and revealed two neutral complexes with their tridentate chelate ligands meridionally coordinated. Completing the coordination spheres of the square-pyramidal structures, a chloride ion occupies the apical position and another is bonded in the basal plane. In addition, complexes **1** and **2** were investigated by infrared, electronic, and EPR spectroscopies, cyclic voltammetry, and potentiometric equilibrium studies. The hydrolytic activity on phosphate diester cleavage of **1** and **2** was investigated utilizing 2,4-BDNPP as substrate. These experiments were carried out at 50 °C, and the data treatment was based on the Michaelis–Menten approach, giving the following kinetic parameters (complex **1**/complex **2**): v_{max} (mol L^{-1} s^{-1}) = $16.4 \times 10^{-9}/7.02 \times 10^{-9}$; K_M (mol L^{-1}) = $17.3 \times 10^{-3}/3.03 \times 10^{-3}$; k_{cat} (s^{-1}) = $3.28 \times 10^{-4}/1.40 \times 10^{-4}$. Complex **1** effectively promoted the hydrolytic cleavage of double-strand plasmid DNA under anaerobic and aerobic conditions, with a rate constant of 0.28 h^{-1} for the decrease of form I, which represents about a 10^7 rate increase compared with the estimated uncatalyzed rate of hydrolysis.

Introduction

Much information about the metal roles in natural systems is currently provided by comparative studies on metalloenzymes and metal compounds. Thus, metalloenzymes such as purple acid phosphatases[1,2] and alkaline phosphatases,[3,4] for which mechanistic studies are available, have been used as a successful starting point in the development of a class of synthetic metal complexes known as synthetic hydrolases and/or chemical nucleases. In the past decade, bioinorganic chemists have been engaged in metallic ion studies related to medical matters, such as the excess or the lack of metal

* Author to whom correspondence should be addressed. Tel: 55-48-331-9219 R226. Fax: 55-48-331-9711. E-mail: ademir@qmc.ufsc.br.
[†] Departamento de Química, Universidade Federal de Santa Catarina.
[§] Universidade Federal do Paraná.
[||] Universidade Federal de São Carlos.
[⊥] Departamento de Bioquímica, Universidade Federal de Santa Catarina.
[‡] Departamento de Física, Universidade Federal de Santa Catarina.

(1) Klabunde, T.; Sträter, N.; Fröhlich, R.; Witzel, H.; Krebs, B. *J. Mol. Biol.* **1996**, *259*, 737−748.
(2) Lindqvist, Y.; Johansson, E.; Kaija, H.; Vihko, P. *J. Mol. Biol.* **1999**, *291*, 135−147.
(3) Holtz, K. M.; Kantrowitz, E. R. *FEBS Lett.* **1999**, *462*, 7−11.
(4) Stec, B.; Hehir, M. J.; Brennan, C.; Nolte, M.; Kantrowtz, E. R. *J. Mol. Biol.* **1998**, *277*, 647−662.

10.1021/ic026277c CCC: $25.00
Published on Web 11/13/2003

ions in biological systems, as well as the development of new drugs.[5] New compounds able to catalytically hydrolyze biomolecules such as proteins, phospholipids, ATP, DNA, and RNA are of current interest. Naturally, nucleases are the enzymes that rapidly hydrolyze the DNA phosphodiester bond by a factor of 10^{12} compared to the noncatalyzed reaction.[6] The first-order rate constants for the phosphodiester hydrolysis of single-stranded and double-stranded DNA have been estimated as 6×10^{-9} and 6×10^{-10} min^{-1}, respectively, under physiological conditions.[7] In addition, the half-life of phosphodiester bonds in DNA has been estimated as 130000 years at 25 °C and neutral pH, whereas in RNA it is only 4000 years under the same conditions.[8] The stability of these phosphodiester bonds indicates the need for the maintenance of the genetic code to use DNA as genetic material.[6,8,9] Although a great number of natural nucleases are known, the search for small molecules able to cleave DNA bonds has been attracting special attention in attempts to identify the mechanism of the cleavage reactions, as well as their applicability as synthetic restriction enzymes, conformational probes, and catalysts. Furthermore, these compounds can aid in the understanding of the metal ion roles in natural systems and the design of more effective synthetic hydrolases.[8] Initially, the chemical nucleases were known as oxidative agents due to their oxidative attack on the ribose ring.[10] In this class of compounds are the complexes 1,10-phenanthroline−copper(II), Fe−EDTA and its derivatives, some metalloporphyrins, octahedral complexes with 4,7-diphenyl-1,10-phenanthroline, and Bleomicin.[6,10] However, these compounds present the inconvenience of the generation of free radicals and fragments that are unable to be enzymatically ligated, which limit its use in molecular biology and genetics. Thus, metal complexes that catalyze the DNA hydrolytic cleavage are of special interest. In order to obtain this kind of complex, a variety of metal complexes have been synthesized and investigated with respect to their ability to hydrolyze small phosphoesters, including complexes with Ni^{II}, Cu^{II}, Zn^{II}, Co^{II}, Fe^{III}, and lanthanide.[11−13] Mononuclear complexes with various ligands have been studied including those with tripods and tridentates amines[14] and with macrocycles.[8,15] Dinuclear complexes have also been employed in the hydrolysis of phosphoesters and DNA, with special attention to be given to the work of Chin and co-workers (complexes with Co^{III} [16] and Cu^{II} [17]), Schnaith and co-workers,[18] Toia and co-workers,[19] and Molenveld and co-workers[20,21] (complexes of Cu^{II} employing calix[4]arene derivatives). Very recently, we reported[22] two new dinuclear complexes with bound hydroxide, one diiron(III), and one dicopper(II), which hydrolytically cleave DNA in the pH range 6.1−8.0. Here we present the syntheses and characterization of two new imidazole tridentate ligands [(2-(imidazol-4-yl)ethyl)(1-methylimidazol-2-yl)methyl]imine (HISMIMI) and its reduced form HISMIMA (Chart 1). These ligands were employed in the syntheses of the mononuclear *cis*-dichloro Cu(II) complexes (**1** and **2**) and in their respective dinuclear complexes (**3** and **4**). All complexes were isolated and characterized by a variety of techniques.

Chart 1. Structure of the Ligands and Complexes

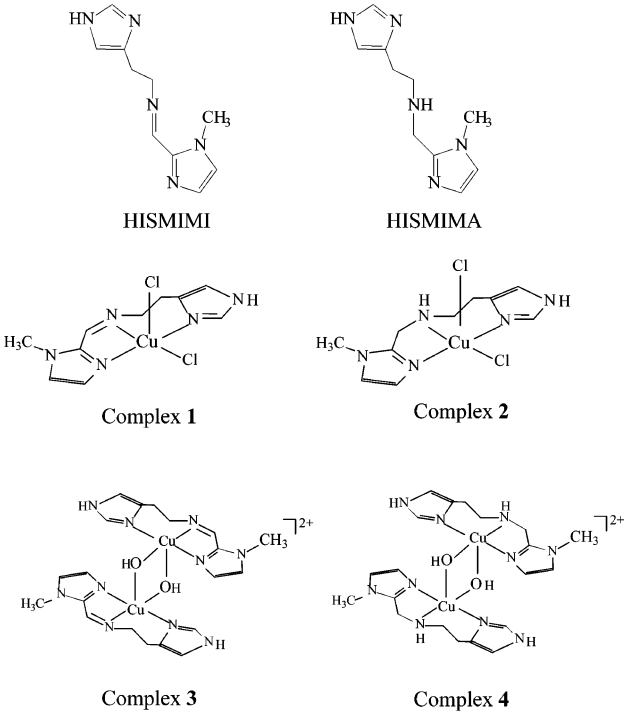

(5) (a) Lippard, S. J. Metals in medicine. In *Bioinorganic Chemistry*; Bertini, I., Gray, H. B., Lippard, S. J., Valentine, J., Eds.; University Science Books: Sausalito, 1994; pp 505−583. (b) Lippard, S. J.; Berg, J. M. *Principles of Bioinorganic Chemistry*; University Science Books: Mill Valley, 1994; pp 175−212.
(6) Sigman, D. S.; Mazumder, A.; Perrin, D. M. *Chem. Rev.* **1993**, *93*, 2295−2316.
(7) Dong, G.; Zeikus, J. G. *Enzyme Microb. Technol.* **1997**, *21*, 335−340.
(8) Hegg, E. L.; Burstyn, J. N. *Coord. Chem. Rev.* **1998**, *173*, 133−165.
(9) Westheimer, F. H. *Science* **1987**, *235*, 1173−1178.
(10) Sigman, D. S. *Biochemistry* **1990**, *29*, 9097−9105.
(11) Chin, *J. Acc. Chem. Res.* **1991**, *24*, 145−152.
(12) Blaskó, A.; Bruice, T. C. *Acc. Chem. Res.* **1999**, *32*, 475−484.
(13) Williams, N. H.; Takasaki, B.; Wall, M.; Chin, J. *Acc. Chem. Res.* **1999**, *32*, 485−493.
(14) (a) Morrow, J. R.; Trogler, W. C. *Inorg. Chem.* **1988**, *27*, 3387−3394. (b) Wahnon, D.; Hynes, R. C.; Chin, J. *J. Chem. Soc., Chem. Commun.* **1994**, 1441−1442. (c) Young, M. J.; Wahnon, D.; Hynes, R. C.; Chin, J. *J. Am. Chem. Soc.* **1995**, *117*, 9441−9447. (d) Itoh, T.; Hisada, H.; Usui, Y.; Fujii, Y. *Inorg. Chim. Acta* **1998**, *283*, 51−60. (e) Liu, C.; Zhou, J.; Li, Q.; Wang, L.; Liao, Z.; Xu, H. J. *Inorg. Biochem.* **1999**, *75*, 233−240. (f) Kurosaki, H.; Tawada, T.; Kawasoe, S.; Ohashi, Y.; Goto, M. *Bioorg. Med. Chem. Lett.* **2000**, *10*, 1333−1337. (g) Ibrahim, M. M.; Shimomura, N.; Ichikawa, K.; Shiro, M. *Inorg. Chim. Acta* **2001**, *313*, 125−136.
(15) (a) Hegg, E. L.; Burstyn, J. N. *Inorg. Chem.* **1996**, *35*, 7474−7481. (b) Deal, K. A.; Burstyn, J. N. *Inorg. Chem.* **1996**, *35*, 2792−2798. (c) Hegg, E. L.; Mortimore, S. H.; Cheung, C. L.; Huyett, J. E.; Powell, D. R.; Burstyn, J. N. *Inorg. Chem.* **1999**, *38*, 2961−2968. (d) Deck, K. M.; Tseng, T. A.; Burstyn, J. N. *Inorg. Chem.* **2002**, *41*, 669−677.
(16) Williams, N. H.; Cheng, W.; Chin, J. *J. Am. Chem. Soc.* **1998**, *120*, 8079−8087.
(17) Chin, J.; Zou, X. *J. Am. Chem. Soc.* **1988**, *110*, 223−225.
(18) Schnaith, L. M. T.; Banson, R. S.; Que, L., Jr., *Proc. Natl. Acad. Sci. U.S.A.* **1994**, *91*, 569−573.
(19) Duboc-Toia, C.; Mégane, S.; Vincent, J. M. *Inorg. Chem.* **1997**, *36*, 6148−6149.
(20) Molenveld, P.; Engbersen, J. F. J.; Kooijman, H.; Spek, A. L.; Reinhoudt, D. N. *J. Am. Chem. Soc.* **1998**, *120*, 6726−6737.
(21) Molenveld, P.; Engbersen, J. F. J.; Reinhoudt, D. N. *Chem. Soc. Rev.* **2000**, *29*, 75−86.
(22) (a) Neves, A.; Terenzi, H.; Hörner, R.; Horn, A., Jr.; Szpoganics, B.; Sugai, J. *Inorg. Chem. Commun.* **2001**, *4*, 388−391. (b) Rossi, L. M.; Neves, A.; Hörner, R.; Terenzi, H.; Szpoganics, B.; Sugai, H. *Inorg. Chim. Acta* **2002**, *337*, 366−370.

Kinetic experiments have demonstrated that complexes **1** and **2** are able to hydrolyze the model substrate 2,4-BDNPP. Moreover, these complexes also show high efficiency in the cleavage of plasmid and genomic DNA in aqueous solution, indicating their potential as chemical nucleases.

Experimental Section

Abbreviations: DTT, DL-dithiothreitol; EDTA, ethylenediaminetetraacetic acid disodium salt; HISMIMI, [(2-(imidazol-4-yl)ethyl)(1-methylimidazol-2-yl)methyl]imine; HISMIMA, [(2-(imidazol-4-yl)ethyl)(1-methylimidazol-2-yl)methyl]amine; 2,4-BDNPP, bis(2,4-dinitrophenyl) phosphate; CHES, 2-[*N*-cyclohexylamino]ethanesulfonic acid; TRIS, tris(hydroxymethyl)aminomethane; [9]aneN$_3$, 1,4,7-triazacyclononane; [10]aneN$_3$, 1,4,7-triazacyclodecane; [11]aneN$_3$, 1,4,8-triazacycloundecane; 2-MeIm$_2$Pro, 1,3-bis(*N*-methylimidazoleimine)propan-2-ol; hfac, hexafluoroacetylacetonate; BMIMA, bis[2-(1-methylimidazole)methyl]amine; L$_1$, [(2-(imidazol-4-yl)ethyl)(1-imidazol-2-yl)methyl]amine; L$_2$, 1-(imidazol-4-yl)-2-[(2-pyridylmethylene)amine]ethane; L$_3$, bis(2-benzimidazoylmethyl)amine; L$_4$, bis(pyridylmethyl)amine; L$_5$, *N*-tris[*N*′-bis(2-pyridylmethyl)aminemethyl]amine; L, *N*,*N*′,*N*″-trimetil-1,4,7-triazacyclononane. HIS, histamine; biap, *N*,*N*-bis(2-ethyl-5-methyl-imidazol-4-yl-methyl)aminepropane.

Materials. 1-Methyl-2-imidazolecarboxaldehyde,[23] bis(2,4-dinitrophenyl) phosphate,[24] and [Cu(CH$_3$CN)$_4$]X (X = ClO$_4^-$ or PF$_6^-$)[25] were synthesized by methods previously described. All other chemicals and solvents were reagent grade purchased from commercial sources and used without further purification. Spectroscopic grade solvents were used in syntheses and characterization of the complexes. Calf thymus (CT) and pUC18 plasmid DNA were purchased from Amersham Biosciences; 18-mer oligonucleotides (poly dA, poly dT, poly dC, or poly dG) were from Gibco BRL; pBSKII plasmid DNA was from Stratagene; pBEND plasmid DNA was a kind gift of Dr. A. Kolb (Institut Pasteur); and mussel genomic DNA (gDNA) was obtained in our laboratory by classical methods as described in the literature.[22] All chemicals used in DNA assays were reagent grade.

Instrumentation. Infrared spectra were recorded on a Perkin-Elmer model 16PC spectrometer, in KBr pellets or film in the 4000−400 cm^{-1} range. ^{1}H NMR spectra were obtained on a Bruker Ac-200F spectrometer in DMSO-d_6 or CDCl$_3$. Elemental analyses were performed on a Carlo Erba Instrument E-1110. Molar conductivities were measured on a Digimed CD-21 condutivimeter at 25 °C. UV−vis spectra were recorded on Perkin-Elmer Lambda 19 spectrometer on MgO pellets or solutions. Cyclic voltammograms were performed with a Princeton Applied Research (PAR) 273 system at room temperature under argon atmosphere. These experiments were carried out employing a standard three-component system: a carbon glass working electrode, a platinum wire auxiliary electrode, and an Ag/AgCl pseudo-reference electrode constructed in our laboratory. To monitor the reference electrode, the ferrocenium−ferrocene couple was used.[26] Cyclic voltammetric experiments involving DNA were performed at 50 °C under argon. EPR spectra were recorded on a Bruker ESP300E spectrometer at room and N$_2$ liquid temperature. Magnetic susceptibility data were obtained from the measured magnetic moment of powder samples of complexes **3** and **4**, over the temperature range 6−300 K, under an applied magnetic field of 0.1 T. Measurements of the magnetic moment were carried out in a Quantum Design MPMS-5 SQUID magnetometer. Diamagnetic corrections were performed using the Pascal tables.[27]

Ligands Syntheses. The Schiff base HISMIMI was synthesized by a condensation reaction between histamine dihydrochloride (3.1 g, 17 mmol), previously neutralized with KOH (1.9 g, 34 mmol), and 1-methyl-2-imidazolecarboxaldehyde in 50 mL of methanol at 0 °C. This solution was stirred at this temperature for 3 h and the solvent removed under reduced pressure, yielding quantitative yellow oil. ^{1}H NMR (DMSO-d_6, 200 MHz): δ 2.83 (t, 2H, J = 7.07 Hz, CH$_2$); 3.78 (t, 2H, J = 7.07 Hz, CH$_2$); 3.98 (s, 3H, CH$_3$); 6.77 (s, 1H, CH$_{Ar}$); 7.01 (s, 1H, CH$_{Ar}$); 7.28 (s, 1H, CH$_{Ar}$); 7.51 (s, 1H, CH$_{Ar}$); 8.19 (s, 1H, HC=N). IR (film, cm^{-1}): 3136−2562 (ν CH); 1656−1442 (ν C=N/C=C); 1102 (ν C−N), 774 (δ CH$_{Ar}$). The corresponding amine (HISMIMA)[28] was obtained by catalytic hydrogenation of the Schiff base HISMIMI in methanolic solution (50 mL), using Pd/C (5%) as catalyst. The reaction mixture was reduced overnight, the catalyst filtered off, and the solvent removed under reduced pressure without heating (yield 2.2 g, 85%).^{1}H NMR (CDCl$_3$, 200 MHz): δ 2.78 (t, 2H, J = 5.7 Hz, CH$_2$); 2.94 (t, 2H, J = 5.7 Hz, CH$_2$); 3.62 (s, 3H, CH$_3$); 3.85 (s, 2H, CH$_2$);6.73 (s, 1H, CH$_{Ar}$); 6.82 (s, 1H, CH$_{Ar}$); 6.91 (s, 1H, CH$_{Ar}$); 7.48 (s, 1H, CH$_{Ar}$). IR (film, cm^{-1}): 3110−2854 (ν CH); 1647−1469 (ν C=N/C=C); 1103 (ν C−N), 749 (δ CH$_{Ar}$).

SAFETY NOTE! Although no problems were encountered during the reduction reaction by catalytic hydrogenation, the catalyst (Pd/C) undergoes spontaneous combustion in methanol and must be handled with care.

Syntheses of Complexes. [Cu(HISMIMI)Cl$_2$] (1). Complex **1** was obtained mixing ethanolic solutions of the HISMIMI ligand (0.20 g, 1 mmol, in 10 mL) and CuCl$_2$·2H$_2$O (0.17 g, 1 mmol, in 10 mL of ethanol), with stirring, at 60 °C for 15 min. After cooling to room temperature, a microcrystalline blue-green solid formed, which was filtered off and washed with cold propan-2-ol alcohol and diethyl ether. Monocrystals suitable for X-ray analysis were obtained by recrystallization in methanol/water (10:1) solution (yield 0.21 g, 62%). (Found: C, 35.43; H, 3.92; N, 20.44. Calcd for CuC$_{10}$H$_{13}$N$_5$Cl$_2$: C, 35.57; H, 3.88; N, 20.74.) Molar conductivity: 142 Ω^{-1} cm^2 mol^{-1} in acetonitrile (1:1 type[29]), which evidences the labilization of one chloride ion. IR (KBr, cm^{-1}): ν (NH) 3136, ν (CH) 3068−2634, ν (C=N$_{imime}$) 1620, ν (C=N/C=C) 1578−1421, ν (C−N) 1087, δ (CH$_{Ar}$) 752.

[Cu(HISMIMA)Cl$_2$]·H$_2$O (2). Complex **2** was synthesized by the same procedure described for complex **1**. Monocrystals for the X-ray crystallographic analysis were obtained from an acetonitrile/water (10:1) solution (yield 0.20 g, 60%). (Found: C, 33.75; H, 4.92; N, 19.83. Calcd for CuC$_{10}$H$_{15}$N$_5$Cl$_2$·H$_2$O: C, 33.58; H, 4.79; N, 19.58.) Molar conductivity: 84 Ω^{-1} cm^2 mol^{-1} in methanol (1:1 type[29]) evidencing the labilization of one chloride ion. IR (KBr, cm^{-1}): ν (OH) 3454, ν (NH) 3218/3120, ν (CH) 3034−2636, ν (C=N/C=C) 1629−1421, ν (C−N) 1078, δ (CH$_{Ar}$) 785.

[Cu$_2$(HISMIMI)$_2$(OH)$_2$](ClO$_4$)$_2$·2H$_2$O (3). Complex **3** was obtained by the two following procedures: (i) to an aqueous solution of complex **1** were added a few drops of NaOH (1 mol L^{-1}) until pH 9.5−10.0 resulting in a deep blue color. To this solution was added 0.5 mmol of NaClO$_4$, yielding a blue solid, which was filtered

(23) Oberhausen, K. J.; Richardson, J. F.; Buchanan, R. M.; Pierce, W. *Polyhedron* **1989**, *8*, 659−668.
(24) Bunton, C. A.; Farber, S. J. *J. Org. Chem.* **1969**, *34*, 767−772.
(25) Kubas, G. J. *Inorg. Synth.* **1979**, *19*, 90−93.
(26) Gagné, R. R.; Koval, C. A.; Lisensky, G. C. *Inorg. Chem.* **1980**, *19*, 2854−2855.
(27) Karlin, R. L. *Magnetochemistry*; Springer-Verlag: Berlin-Heidelberg, 1986; p 3.
(28) Scarpellini, M.; Neves, A.; Bortoluzzi, A. J.; Joussef, A. C. *Acta Crystallogr., Sect. C* **2001**, *C57*, 356−358.
(29) Geary, W. J. *Coord. Chem. Rev.* **1971**, *7*, 81−122.

off and washed with cold propan-2-ol alcohol and diethyl ether. (ii) A dry methanolic solution of HISMIMA (0.21 g, 1 mmol, in 10 mL) was added to a dry acetonitrile solution of $[Cu(CH_3CN)_4]$-ClO_4 (0.32 g, 1 mmol, in 10 mL), under an argon atmosphere with stirring at room temperature. The resulting yellow solution was stirred for 10 min and then submitted to O_2 flow for 5 min, affording a deep blue color. To this solution was added 5 mL of propan-2-ol alcohol. The slow evaporation of the solvents yields blue microcrystals (yield 0.21 g, 62%). (Found: C, 29.29; H, 3.87; N, 16.80. Calcd for $Cu_2C_{20}H_{28}N_{10}O_{10}Cl_2 \cdot 2H_2O$: C, 29.93; H, 4.02; N, 17.45.) Molar conductivity: 221 Ω^{-1} cm^2 mol^{-1} in acetonitrile (2:1 type[29]). IR (KBr, cm^{-1}): ν (OH) 3398, ν (NH) 3270/3138, ν (CH) 2950−2885, ν (C═N_{imime}) 1630, ν (C═N/C═C) 1590−1436, ν (ClO_4) 1096, δ (CH_{Ar}) 624.

$[Cu_2(HISMIMA)_2(OH)_2](ClO_4)_2 \cdot {}^1/_2CH_3CN$ (4). Complex **4** was synthesized by the same procedures described above for complex **3** (yield 0.40 g, 52%). (Found: C, 32.12; H, 4.12; N, 18.04. Calcd for $Cu_2C_{20}H_{32}N_{10}O_{10}Cl_2 \cdot {}^1/_2CH_3CN$: C, 31.88; H, 4.27; N, 18.59.) Molar conductivity: 304 Ω^{-1} cm^2 mol^{-1} in acetonitrile (2:1 type[29]). IR (KBr, cm^{-1}): ν (OH) 3616/3539, ν (NH) 3242/3125, ν (CH) 2949−2864, ν (C═N/C═C) 1619−1428, ν (ClO_4) 1091, δ (CH_{Ar}) 749.

CAUTION! Perchlorate salts with organic ligands are potentially explosive and should be handled in small quantities with care.

Potentiometric Equilibrium Studies. The potentiometric studies were carried out with a Micronal B375 pH meter fitted with blue-glass and calomel reference electrodes calibrated to read $-\log [H^+]$ directly, designated as pH. Bidistilled water in the presence of $KMnO_4$ was used to prepare the water solutions. The electrode was calibrated using the data obtained from a potentiometric titration of a known volume of a standard 0.100 mol L^{-1} HCl solution with a standard 0.100 mol L^{-1} KOH solution. The ionic strength of the HCl solution was maintained at 0.100 mol L^{-1} by addition of KCl. The measurements were carried out in a thermostated cell containing a complex solution (0.05 mol/50 mL) with ionic strength adjusted to 0.100 mol L^{-1} by addition of KCl, at 25.00 ± 0.05 °C. The experiments were performed under an argon flow to eliminate the presence of atmospheric CO_2. The samples were titrated by addition of fixed volumes of a standard CO_2-free KOH solution (0.100 mol L^{-1}). Computations were carried out with the BEST program, and species diagrams were obtained with SPE and SPEPLOT programs.[30]

Kinetics Procedures. Hydrolysis kinetics experiments of bis-(2,4-dinitrophenyl)phosphate (2,4-BDNPP)[24] were monitored spectrophotometrically at 400 nm, due to the 2,4-dinitrophenolate absorption as the product released during the reaction. The 2,4-dinitrophenolate concentration was calculated from the molar extinction coefficient (ϵ = 19100 mol^{-1} L cm^{-1}).[20] Reactions were monitored to less than 5% of conversion of substrate to product, and the data were treated by the initial rate method. Initial rates were directly obtained from the plot of 2,4-dinitrophenolate concentration vs time. The effect of the pH on the hydrolysis of 2,4-BDNPP was studied by using an excess of complex. In these experiments, the solutions of the complexes were prepared by diluting complex stock solution (50×10^{-3} mol L^{-1} in water), in the appropriate buffer at the desired pH at 50 °C (I = 0.1 mol L^{-1} with KCl). Reactions were prepared in parallel to ensure identical conditions of concentration and ionic strength. In a typical run, 100 μL of a stock solution of 2,4-BDNPP in methanol (50×10^{-3} mol L^{-1}) was added to 4 mL of the reaction solution in the thermostated cell carriage of a HP spectrophotometer, which was operating on-line with a computer. Kinetic studies involving the dependence of the reaction rate on the complex concentration were carried out at the respective saturation pH of each complex. These experiments were performed from solutions of complexes prepared by dilutions of stock solutions (50×10^{-3} mol L^{-1} in water), in the desired buffer, at 50 °C (I = 0.1 mol L^{-1} with KCl). The experiments involving the substrate effects were performed at the respective saturation pH of each complex in analogous conditions as described above. Substrate solutions were freshly prepared in the appropriate buffer, at 50 °C (I = 0.1 mol L^{-1} with KCl). In the experiments, in which the substrate concentration exceeded the complex concentration, correction for the spontaneous hydrolysis of the phosphate diester was accomplished by direct difference using a reference cell under identical conditions without adding the catalyst.

DNA Cleavage. DNA cleavage was performed as described.[22] DNA cleavage products were separated by agarose gel electrophoresis and visualized in a UV-transilluminator (FLX −20 Vilber Loumart). The gel was photographed (Sony Digital still camera MVC FD75), and the bands on the gel were quantified using the Scion Image Software (Scion Corp.).

Anaerobic Reactions. Deoxygenated water was prepared by a two-step procedure. First, water was submitted to agitation under vacuum until complete elimination of air bubbles; and the water was then equilibrated with argon to aid in the deoxygenation process. The water was stored under an argon atmosphere prior to use. All solutions and reaction mixtures used were prepared in an argon-filled glovebag. Samples were then incubated at 50 °C in a sealed argon-filled vacuum desiccator. After a 24 h incubation period reactions were stopped as in the aerobic experiments. All other conditions and procedures were the same as those for aerobic reactions.

Single-Crystal X-ray Structure Determination. The intensity data for complexes **1** and **2** were collected with an Enraf-Nonius CAD4 diffractometer, at room temperature, with graphite-monochromated Mo Kα radiation. The unit cell parameters were determined on the setting angles of 25 centered reflections. All data were corrected for Lorentz and polarization effects. Empirical absorption correction based on the azimuthal scans of 7 appropriate reflections was also applied to the collected intensities through the PLATON program.[31a] The structure was solved by direct methods and refined by full-matrix least-squares methods using SHELXS97[31b] and SHELXL97[31c] programs, respectively. All non-hydrogen atoms were refined anisotropically. H atoms attached to C atoms were placed at their idealized positions, with C−H distances and U_{eq} values taken from the default settings of the refinement program. H atoms bonded to N and O atoms were found from difference the Fourier map, and these atoms were treated using a riding model. The figures of the molecular structures were produced with the ZORTEP program.[31d] Further crystal structure and refinement data for complexes **1** and **2** are summarized in Table 1.

Results and Discussion

Syntheses of Ligands and Copper(II) Complexes. The tridentate imidazole ligands were synthesized by standard

(30) Martell, A. E.; Motekaits, R. J. *Determination and use of stability constants*; VHC Publishers: New York, 1992.

(31) (a) Spek, A. L. *Acta Crystallogr., Sect. A* **1990**, *36*, C34. (b) Sheldrick, G. M. *SHELXS 97, Program for the Solution of Crystal Structures*; University of Göttingen: Göttingen, Germany, 1997. (c) Sheldrick, G. M. *SHELXL 97, Program for the Refinement of Crystal Structures*; University of Göttingen: Göttingen, Germany, 1997.(d) Zolnai, L. *ZORTEP. An interactive ORTEP program*; University of Heidelberg: Heidelberg, Germany, 1997.

Table 1. Summary of Crystallographic Data for Complexes **1** and **2**

	complex **1**	complex **2**
formula	$C_{10}H_{13}Cl_2CuN_5$	$C_{10}H_{17}Cl_2CuN_5O$
fw	337.69	357.73
T (K)	293(2)	293(2)
λ (Å)	0.71073	0.71073
crystal system	triclinic	triclinic
space group	$P\bar{1}$	$P\bar{1}$
a (Å)	8.169(2)	6.828(1)
b (Å)	11.857(2)	8.559(2)
c (Å)	14.069(3)	13.548(3)
α (deg)	99.17(3)	73.75(3)
β (deg)	95.57(3)	84.78(3)
γ (deg)	93.19(3)	72.69(3)
V (Å^3)	1335.4(5)	725.7(3)
Z	4	2
μ (mm^{-1})	2.024	1.872
ρ_{calc} (g/cm^3)	1.680	1.637
reflns	5115	2867
unique	4860 (R_{int} = 0.0109)	2673 (R_{int} = 0.0081)
params	328	171
ext coeff	0.0298(9)	0.046(2)
GOF (F^2)	1.044	1.120
$R(F)^a$ ($I > 2\sigma(I)$)	0.0267	0.0248
$R_w(F^2)^b$ (all data)	0.0760	0.0704

^{a} $R(F) = \sum||F_o| - |F_c||/\sum|F_o|$. ^{b} $R_w(F^2) = \{\sum[w(F_o^2 - F_c^2)^2/\sum[w(F_o^2)^2]\}^{1/2}$.

methods of Schiff base preparation (HISMIMI), followed by the catalytic hydrogenation reaction in order to obtain the amine HISMIMA. Both ligands were obtained in a purity grade for use without further purification. These ligands were able to coordinate to the copper(II) ion yielding both mono- and dinuclear complexes. The mononuclear dihalo complexes **1** and **2** were obtained in good yields by reacting stoichiometric amounts (1:1) of $CuCl_2 \cdot H_2O$ and the corresponding ligands HISMIMI and HISMIMA. The dinuclear $[Cu_2(HISMIMI)_2(OH)_2](ClO_4)_2$ and $[Cu_2(HISMIMA)_2(OH)_2](ClO_4)_2$ complexes were obtained in basic medium (pH ∼ 10) by adding NaOH and $NaClO_4$ to an aqueous solution of **1** and **2**, respectively. Complexes **1** and **2** can be obtained as adequate crystals for X-ray crystallography when recrystallized from CH_3OH/water (10:1) and CH_3CN/water (10:1), respectively. Conductivity measurements in CH_3CN solution for **3** and **4**, determined at 25 °C, are in the range 220−300 Ω^{-1} cm^2 mol^{-1}, indicating their 2:1 electrolyte behavior,[29] consistent with the formula from elemental analysis.

X-ray Structural Characterization. Complex **1** crystallizes as light blue single crystals that belong to the triclinic system, space group $P\bar{1}$. A Zortep[31d] view of the complex is shown in Figure 1. The main angles and bond distances are presented in Table 2. The crystalline structure of complex **1** shows the presence of two crystallographically independent molecules (**1a** and **1b**) in the asymmetric unit. These molecules are geometrical isomers with two distinct conformational configurations in the six-membered rings that arise from the histamine residue coordination. In complex **1**, the Cu^{II} ion is coordinated to two chloride ions and to three nitrogen atoms from the HISMIMI ligand, in which the imine form is characterized by a typical C=N[32] Schiff base bond length (Table 2). The geometry around the metal

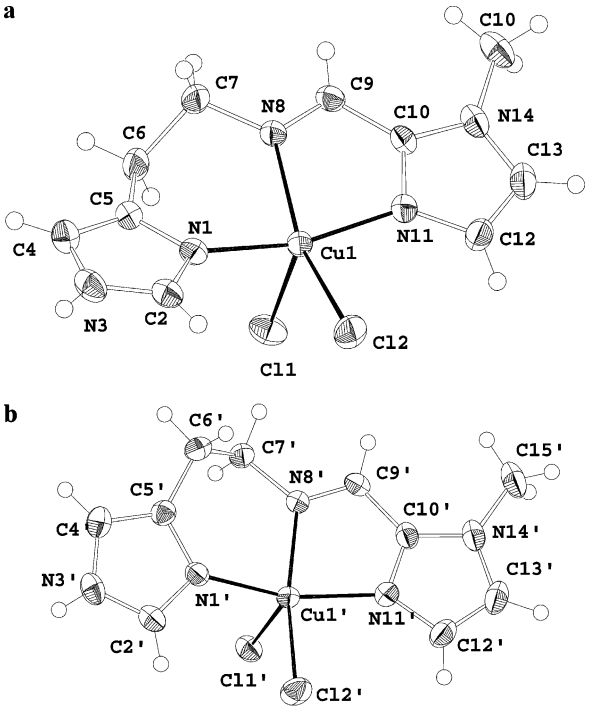

Figure 1. View of the complex Cu(HISMIMI)Cl_2 **1**: molecule 1 (above) and molecule 2 (bottom), with atom-labeling scheme and ellipsoids at 40% probability.

Table 2. Selected Bond Lengths (Å) and Angles (deg) for Complex **1**

Cu1−N1	1.9596(19)	Cu1′−N1′	1.975(2)
Cu1−N11	1.9872(19)	Cu1′−N11′	1.992(2)
Cu1−N8	2.096(2)	Cu1′−N8′	2.063(2)
Cu1−Cl2	2.2882(11)	Cu1′−Cl2′	2.2930(11)
Cu1−Cl1	2.5789(10)	Cu1′−Cl1′	2.5705(10)
N8−C9	1.268(3)	N8′−C9′	1.269(3)
N1−Cu1−N11	166.00(8)	C7−N8−Cu1	125.55(15)
N1−Cu1−N8	89.63(8)	N1′−Cu1′−N11′	161.70(8)
N11−Cu1−N8	79.09(8)	N1′−Cu1′−N8′	90.18(8)
N1−Cu1−Cl2	94.55(6)	N11′−Cu1′−N8′	79.79(8)
N11−Cu1−Cl2	92.81(6)	N1′−Cu1′−Cl2′	93.78(6)
N8−Cu1−Cl2	157.25(6)	N11′−Cu1′−Cl2′	92.29(6)
N1−Cu1−Cl1	92.58(6)	N8′−Cu1′−Cl2′	164.88(6)
N11−Cu1−Cl1	97.31(6)	N1′−Cu1′−Cl1′	95.23(6)
N8−Cu1−Cl1	98.90(6)	N11′−Cu1′−Cl1′	100.40(6)
Cl2−Cu1−Cl1	103.22(4)	N8′−Cu1′−Cl1′	92.38(6)
C9−N8−C7	119.8(2)	Cl2′−Cu1′−Cl1′	101.77(4)
C9−N8−Cu1	114.47(16)	N8′−C9′−C10′	114.0(2)

center is best described as slightly distorted square pyramidal in both molecules (τ = 0.05 for **1a** and τ = 0.14 for **1b**) based on the Addison[33] analysis, where τ = 0.0 describes a perfect square pyramid and τ = 1.0 a trigonal bypyramid. In molecule **1a**, the Cu^{II} ion is 0.2965(9) Å above the basal plane, whereas in the molecule **1b** it is displaced by 0.2728(9) Å. Since the bond lengths and angles around the copper center are similar in the two molecules, only the parameters of molecule **1a** will be discussed here. The basal plane is composed of N11, N1, N8, and Cl2 atoms, where the N8 imine nitrogen is in the trans position with respect to the Cl2 ion. The Cl1 chloride ion is apically coordinated at 2.5789(10) Å and completes the metal coordination sphere. The Cu^{II}−N_{imine} bond distance [Cu1−N8: 2.096(2) Å] is in

(32) Vencato, I.; Neves, A.; Scarpellini, M.; Correia, V. R. *Acta Crystallogr., Sect. C* **1998**, *C54*, 97−99.

(33) Addison, A. W.; Rao, T. N.; Reedijk, J.; Vanrijn, J.; Verschoor, G. C. *J. Chem. Soc., Dalton Trans.* **1984**, 1349−1356.

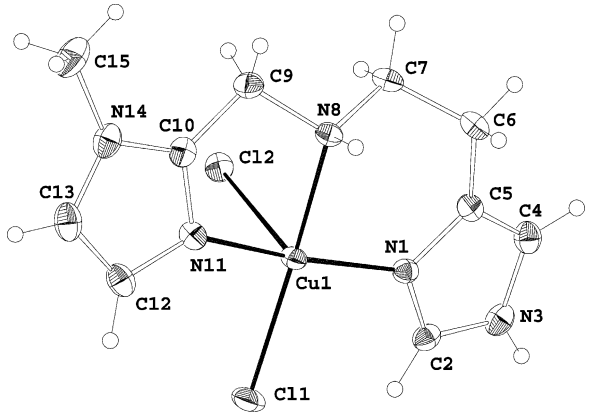

Figure 2. View of the complex Cu(HISMIMA)Cl_2·H_2O **2** with atom-labeling scheme and ellipsoids at 40% probability.

Table 3. Selected Bond Lengths (Å) and Angles (deg) for Complex **2**

Cu1−N11	1.9540(19)	Cu1−Cl1	2.2875(8)
Cu1−N1	1.9662(18)	Cu1−Cl2	2.9242(11)
Cu1−N8	2.0784(17)		
N11−Cu1−N1	171.34(7)	N8−Cu1−Cl1	169.64(5)
N11−Cu1−N8	80.98(8)	N11−Cu1−Cl2	94.31(7)
N1−Cu1−N8	91.93(8)	N1−Cu1−Cl2	90.32(6)
N11−Cu1−Cl1	91.56(7)	N8−Cu1−Cl2	87.57(6)
N1−Cu1−Cl1	94.82(6)	Cl1−Cu1−Cl2	100.23(4)

the middle range of Cu^{II}−N bonds observed for Cu^{II} complexes with Schiff bases: $[Cu(2\text{-}MeIm_2Pro)(H_2O)]^{2+}$, 1.993 Å;[34] $[Cu(hfac)(L_1)M(hfac)_2(L_1)(hfac)Cu]$, M = Zn, 2.031 Å, and M = Cu, 2.033 Å;[35] and $[Cu_2(L_2)_2(N_3)_2]^{2+}$, 2.023 Å.[36] The $Cu-N_{imidazole}$ bond distances [Cu1−N1, 1.9596(19), and Cu1−N11, 1.9872 (19) Å] are the shortest of the coordination sphere, but similar to those observed in some Cu^{II} complexes containing imidazole rings: $[Cu(2\text{-}MeIm_2Pro)(H_2O)]^{2+}$, 1.993(2)/1.992(3) Å;[34] $[Cu(hfac)(L_1)M(hfac)_2(L_1)(hfac)Cu]$, M = Zn, 1.967(4) Å;[35] and $[Cu_2(L_2)_2(N_3)_2]^{2+}$, 1.969(4) Å;[36] $[(L_3)\text{-}Cu(OP(O)(OCH_3)_2)(HOCH_3)]^+$, av 1.963 Å,[14c] and $[Cu(B\text{-}MIMA)(CH_3COO)]^+$, av 1.971 Å.[23] As expected, the Cu−Cl bond lengths are the longest of the coordination sphere [Cu1−Cl1, 2.579(1) Å, and Cu1−Cl2, 2.288(1) Å] and comparable to those reported for other mononuclear *cis*-dihalo Cu^{II} complexes: $Cu([9]aneN_3)Cl_2$, 2.268(1)/2.312(1) Å;[37] $Cu([10]aneN_3)Br_2$, 2.460(2)/2.449(2) Å;[15b] $Cu([11]aneN_3)Br_2$, 2.431(2)/2.491(2) Å;[15b] and $[CuL_4(Cl)_2]$, 2.603(2)/2.267(2) Å.[14c]

Complex **2** crystallizes as blue single crystals that belong to the triclinic crystalline system and space group $P\bar{1}$. A Zortep[31d] view of the complex is shown in Figure 2. The main angles and bond distances are presented in Table 3. The crystalline structure of complex **2** shows similarities with those presented by complex **1**. As can be observed, the Cu^{II} ion lies in a N_3Cl_2 coordination environment composed of two chloride ions and three nitrogen atoms from the HISMIMA ligand, which is coordinated in a meridional fashion, as observed for complex **1**. Complex **2** also shows a square-pyramidal geometry, which is evidenced by the Addison[33] analysis ($t = 0.028$). The basal plane is composed of the N11, N1, N8, and Cl1 atoms, and the Cu^{II} ion lies at 0.1180(8) Å above this plane. In the equatorial plane, the [N1 and N11] imidazole nitrogen atoms are in trans positions with respect to each other and mutually cis to the [N8] amine nitrogen atom and to the [Cl1] chloride. Completing the metal coordination sphere, the Cl2 chloride ion is apically coordinated at 2.9242 (11) Å. The $Cu^{II}-N_{amine}$ bond distance [Cu1−N8: 2.0784(17) Å] is in the range of those reported for Cu^{II} complexes with tridentate amines, in which the amine nitrogen atom lies in the basal plane of a square-pyramidal geometry: $Cu([9]aneN_3)Cl_2$, av 2.051 Å;[37] $Cu([10]aneN_3)Br_2$, av 2.044 Å;[15b] $[Cu(B\text{-}MIMA)(CH_3COO)]^+$, av 2.047(2) Å;[23] $Cu_3(L_5)(NO_3)_2(H_2O)_3]^{4+}$, Cu1−N2 = 2.041(8) and Cu3−N8 = 2.055(8) Å;[38] $[Cu(HISMIMA)(HIS)]^{2+}$, 2.082(3) Å;[28] and $[(L_3)\text{-}Cu(OP(O)(OCH_3)_2)(HOCH_3)]^+$, 2.101(4) Å.[36] The $Cu-N_{imidazole}$ bond lengths [Cu1−N1, 1.9662(18), and Cu1−N11, 1.9540(19) Å] are the shortest of the coordination sphere. This fact reflects the greater π ligand ability of the imidazole rings when compared to the σ donor second amine. These values are similar to those observed in complex **1** and in analogous complexes ($[Cu(HISMIMA)(HIS)]^{2+}$, av 1.980 Å;[28] $[Cu(biap)Br_2]$, av 1.959 Å;[39] and $[Cu(biap)(NO_2)_2]$, av 1.961 Å)[39] and are also similar to the corresponding $Cu-N_{imidazole}$ bonds observed in the complexes mentioned above.[14c,23,34]

Potentiometric Equilibrium Determinations. It is well-known that *cis*-dihalo Cu^{II} complexes generate *cis*-diaqua Cu^{II} complexes in aqueous solutions. Potentiometric titrations of **1** (Figure 3) and **2** (Figure S1, Supporting Information) were therefore carried out and indicated one titratable proton for each pK_a value of 8.9 and 9.3, respectively. The constants of molecule deprotonation were calculated using the BEST7[30] computation program. These values are similar to that determined for the $[LCuCl_2]$ complex[14c] [L = bis(pyridylmethyl)amine)] and are consistent with the dissociation of the equatorial metal-bound water molecule since this should be more acidic than the axially coordinated water molecule. In addition, this result is also in full agreement with the X-ray data of **1** and **2**, which show that the equatorial Cu−Cl bond distances are significantly shorter than the corresponding axial Cu−Cl distances. From this information, we suggest that deprotonation of the equatorial coordinated water molecule in **1** and **2** generates the $[Cu(HISMIMI(H_2O)(OH)]^+$ and $[Cu(HISMIMA(H_2O)(OH)]^+$ molecules as the catalysts for the hydrolysis of phosphate diesters. However, it should be noted that because of the mononuclear−dinuclear equilibrium (**1** ⇔ **3** and **2** ⇔ **4**), the pK_a determined via titration is not simply the pK_a of the coordinated water molecule; it is, however, the kinetically relevant pK_a (vide

(34) Doman, T. N.; Richardson, J. F.; Arar, L.; Buchanan, R. M. *Inorg. Chim. Acta* **1989**, *159*, 219−224.
(35) Colacio, E.; Domínguez-Vera, J. M.; Ghazi, M.; Kivekas, R.; Klinga, M.; Moreno, J. M. *Inorg. Chem.* **1998**, *37*, 3040−3045.
(36) Matsumoto, K.; Ooi, S.; Nakatsuda, K. *J. Chem. Soc., Dalton Trans.* **1985**, 2095−2100.
(37) Schwindinger, W. F.; Fawcett, T. G.; Lalancette, R. A.; Schugar, H. J.; Potenza, J. A. *Inorg. Chem.* **1980**, *19*, 1379−1381.
(38) Frey, S. T.; Sun, H. H. J.; Murty, N. N.; Karlin, K. D. *Inorg. Chim. Acta* **1996**, *242*, 329−338.
(39) Beretta, M.; Bouwman, E.; Casella, L.; Douziech, B.; Driessen, W. L.; Gutierrez-Soto, L.; Monzani, E.; Reedijk, J. *Inorg. Chim. Acta* **2000**, *310*, 41−50.

Table 4. CV Results vs Fc^+/Fc for Complexes **1**, **2**, and **4** in Different Media[a]

complex	medium	E_{pc}	E_{pa}	$E_{1/2}$
1	CH_2Cl_2	−0.676		
	CH_3OH	−0.553/−1.263		
	CH_3OH (pH_{ap} 9)	−1.207		
2	CH_2Cl_2	−0.818		
	CH_3OH	−0.655	−0.485	−0.570
	CH_3OH (pH_{ap} 7.8)	−0.629/−0.911	−0.531	−0.580
	CH_3OH (pH_{ap} 8.8)	−0.934		
4	CH_3CN	−0.999	−0.419	

[a] Reference electrode: Ag/AgCl. Auxiliary electrode: platinum. Working electrode: glassy carbon. Supporting electrolyte: $TBAPF_6$ (0.1 mol L^{-1}). Standard reference: ferrocenium/ferrocene.

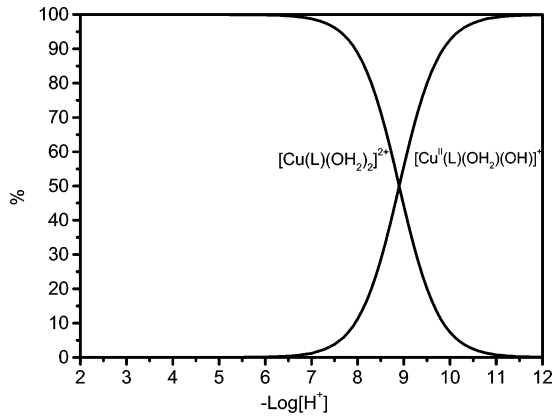

Figure 3. Species distribution curves for complex **1** as a function of −log $[H^+]$, where pK_a value is 8.9.

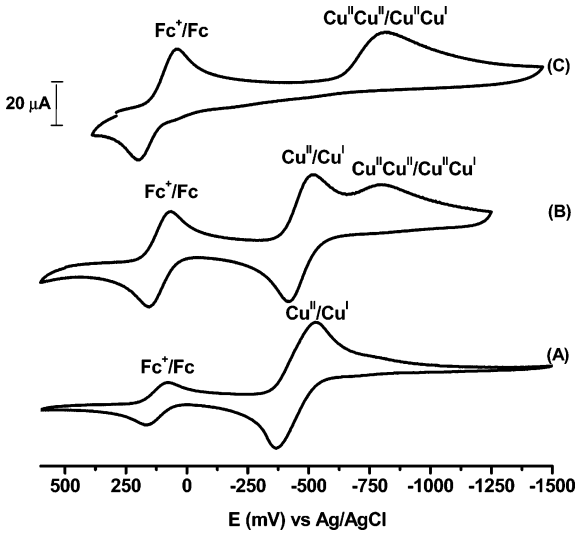

Figure 4. Cyclic voltammograms of complex **2** in methanolic solution (0.1 mol L^{-1} $TBAPF_6$ supporting electrolyte, platinum working electrode, platinum wire auxiliary electrode): (A) pure CH_3OH, (B) $pH_{apparent}$ 7.8, and (C) $pH_{apparent}$ 8.8, at scan rate 100 mV s^{-1}.

infra). A similar conclusion has been drawn by Burstyn et al.[8] for the related $[Cu[9]ane(OH_2)_2]^{2+}$ complex.

Cyclic Voltammetry. Cyclic voltammograms of complexes **1** and **2** were recorded in methanol and dichloromethane solutions, with $TBAPF_6$ as the supporting electrolyte in the potential range +0.6 to −1.5 V vs SCE. The results are summarized in Table 4, and typical voltammograms of **2** are displayed in Figure 4. The studies in dichloromethane were carried out in order to investigate the

Table 5. Absorption Spectral Data for Complexes **1**−**4**

complex	λ_{max} (nm) solid[a]	λ_{max}/nm (ϵ/mol L^{-1} cm^{-1}) organic solvent	water
1	712/800(sh)/378	646 (99)[c,d]	655 (15)[f]
2	670/780(sh)	632 (76)[b,d]	644 (71)[f]
3	620/715(sh)/352	594 (185)[c,d]	
4	582/326	582 (193)[c,d]	

[a] In MgO. [b] In CH_3OH ($C = 8.6 \times 10^{-5}$ mol L^{-1}). [c] In CH_3CN. [d] $C = 1.0 \times 10^{-3}$ mol L^{-1}. [e] $C = 1.1 \times 10^{-3}$ mol L^{-1}. [f] $C = 4.0 \times 10^{-3}$ mol L^{-1}. [g] $C = 5.0 \times 10^{-3}$ mol L^{-1}. [h] $C = 2.0 \times 10^{-3}$ mol L^{-1}.

species containing the chloride ligands in the first coordination sphere of the Cu^{II} centers, whereas the experiments in methanol aimed to characterize the mononuclear species with coordinated water molecules in equilibrium with its corresponding dinuclear complex. The cyclic voltammograms of **1** and **2** in CH_2Cl_2 exhibit a single irreversible reduction wave at −0.68 and −0.82 V vs Fc^+/Fc, respectively, which can be attributed to the $Cu^{II} \rightarrow Cu^{I}$ redox process within mononuclear *cis*-dihalo species. In pure methanol solution, complex **2** shows a single quasi-reversible wave ($\Delta E_p = 170$ mV, Figure 4A) at −0.57 V vs Fc^+/Fc again assigned to the $Cu^{II} \rightarrow Cu^{I}$ redox process of the mononuclear $[Cu(HISMIMA)X_2]$ (X = H_2O or CH_3OH) complex. However, with addition of aqueous NaOH ($pH_{app} = 7.8$) an additional more cathodic irreversible wave (Figure 4B) at −0.911 V appears. We tentatively attribute this wave as being the one electron reduction involving the $Cu^{II}Cu^{II} \rightarrow Cu^{II}Cu^{I}$ couple which results from the equilibrium mononuclear−dinuclear species. In fact, this attribution is supported by the cyclic voltammogram results obtained in CH_3OH with further addition of aqueous NaOH ($pH_{app} = 8.8$), where a single wave (Figure 4C) at −0.934 V vs Fc^+/Fc was observed and by the cyclic voltammogram of the $[Cu_2(HISMIMA)_2(OH)_2]^{2+}$ complex which shows also a single irreversible reduction wave at −0.94 V under identical experimental conditions. The electrochemical behavior of **1** in the water/MeOH solution is identical to that observed for complex **2** (Figure S2, Supporting Information) but with the wave assigned to the mononuclear species being irreversible. From this information it seems reasonable to assume that in aqueous basic solution the mononuclear H_2O/OH^- complexes of **1** and **2** are in equilibrium with their dinuclear $Cu(\mu\text{-}OH)_2Cu$ counterparts in agreement with the solid-state structures proposed for **3** and **4**.

Electronic and EPR Spectroscopies. The UV−vis and EPR measurement conditions and their results for complexes **1**−**4** are shown in Table 5. The electronic spectra, in the solid state, of complexes **1**−**3** display a band in the range of 600−700 nm and a shoulder around 850 nm. For complex **4** only one band located at 582 nm was observed. The electronic absorption spectra for pentacoordinated copper(II) complexes usually fall into two categories.[40] Square-pyramidal complexes typically show a high-energy absorption band in the visible region with a low-energy shoulder.

(40) (a) Lever, A. B. P. *Inorganic Electronic Spectroscopy*; Elsevier Science Publishers B.V.: Amsterdam, 1984; pp 553−572. (b) Ranjedran, U.; Viswanathan, R.; Palaniandavar, M.; Laskiminaraya, N. *J. Chem. Soc., Dalton Trans.* **1994**, 1219−1226.

Table 6. EPR Measurement Conditions and Results for Complexes **1**−**4**

complex	medium	$g_\perp$	$g_\parallel$	$A_\parallel$ ($\times 10^{-4}$ cm^{-1})	$g_\parallel/A_\parallel$
1	solid (rt[c])	2.080	2.300	167.0	137.7
	solid (77 K)	2.080	2.290	166.0	137.9
	DMSO-d_6 (77 K)	2.069	2.245	160.0	140.3
	ethanol/H_2O (77 K)	2.062	2.240	164.5	136.2
	ethanol/buffer(8.9)[a] (77 K)	2.075	2.240	178.0	125.8
2	solid (rt)	2.106	2.290	159.0	144.0
	solid (77 K)	2.102	2.280	150.0	152.0
	DMSO-d_6 (77 K)	2.092	2.240	170.0	131.8
	ethanol/H_2O (77 K)	2.080	2.258	159.0	142.0
	ethanol/buffer (9.3)[b] (77 K)	2.100	2.250	178.0	126.4
3	solid (rt)	$g_{iso} = 2.110$			
	solid (77 K)	$g_{iso} = 2.100$			
	DMSO-d_6 (77 K)	$g_{iso} = 2.115$			
4	solid (rt)	$g_{iso} = 2.100$			
	solid (77 K)	$g_{iso} = 2.098$			
	DMSO-d_6 (77 K)	$g_{iso} = 2.085$			
	CH_3CN	$g_{iso} = 2.080$			

[a] Buffer Trizma−complex **1**: pH = 8.9. [b] Buffer CHES−complex **2**: pH = 9.3. [c] Room temperature.

In contrast, trigonal-bipyramidal complexes have a low-energy absorption band with a high-energy shoulder in the visible region.[40] Therefore, complexes **1**−**3** show spectral features of square-pyramidal geometry, which suggests that it is the geometric arrangement adopted by the Cu^{II} centers in these complexes in the solid state. This is in agreement with the X-ray analysis for complexes **1** and **2**, where a distorted square-pyramidal geometry was observed, as discussed above. In solution (Table 5), all complexes show only a broad ligand field band in the range 580−650 nm. This behavior is characteristic of tetragonally distorted octahedral complexes and suggests that solvent molecules occupy the vacancy positions in the first metal coordination spheres, when the complexes are dissolved.

In the solid state, at room and liquid N_2 temperatures, the mononuclear complexes **1** and **2** exhibit EPR spectra with rhombic symmetry ($g_\parallel > g_\perp$; see Table 6) having a $d_{x^2}-d_{y^2}$ ground state in agreement with the square-pyramidal arrangement observed in the X-ray structure of the complexes. The spectra of **1** in d_6-DMSO, ethanol/water (1:1), and ethanol/CHES buffer (1:1) (pH 8.9), at 77 K, show EPR parameters characteristic of a ligand field force increasing in this order of solvents, as shown by the $g_\parallel/A_\parallel$ ratio (Table 6). The same experiments for complex **2** show the increasing ligand field order in the sequence ethanol/water (1:1), d_6-DMSO, and ethanol/CHES buffer (1:1) (pH 9.3) as also shown by the $g_\parallel/A_\parallel$ ratio (Table 6). EPR spectra obtained from frozen solution samples of **1** and **2** (ethanol/buffer, pH = 8.9−9.3, Figure 5) revealed an additional signal at "half-field" (∼1500 G). This feature can be assigned to the forbidden $\Delta M_S = \pm 2$ transition and is characteristic of dinuclear $Cu^{II}Cu^{II}$ species with a weak antiferromagnetic coupling. In addition, for complex **1**, seven copper hyperfine lines with an average hyperfine spacing of 82 G (one-half that expected for a mononuclear Cu^{II} complex) are clearly visible at $g \cong 4.3$. It should be noted that an idealized spectrum for an axial $Cu^{II}Cu^{II}$ dimer consists of seven hyperfine lines and there is no zero-field splitting for the $\Delta M_S = \pm 2$ transition.[41b] Again, these observations are in agreement with the existence of the mononuclear−dinuclear equilibrium (**1** ⇔ **3** and **2** ⇔ **4**) in solution, under these experimental conditions. Unfortunately we were unable to obtain the EPR spectra of **3** and **4** in frozen ethanol/buffer solution due to the low solubility of the complexes in this medium. In the solid state, at room temperature or 77 K, only broad spectra centered at $g = 2.10-2.11$ were obtained for **3** and **4**, which are in agreement with an antiferromagnetic interaction between the two copper ions in the proposed dinuclear species.[41]

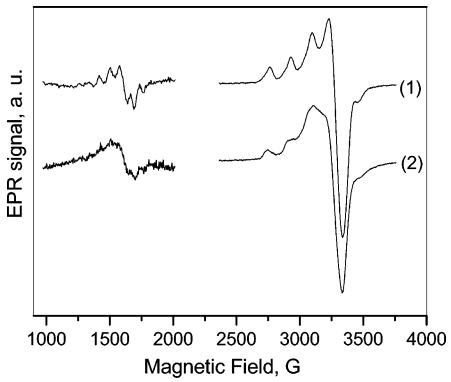

Figure 5. Experimental EPR spectra of complexes **1** (top) and **2** (bottom), in N_2 liquid frozen solutions (ethanol/CHES buffer (1:1) (pH 8.9)) for **1** and ethanol/CHES buffer (1:1) (pH 9.3) at the $g \sim 2$ and $g \sim 4$ regions.

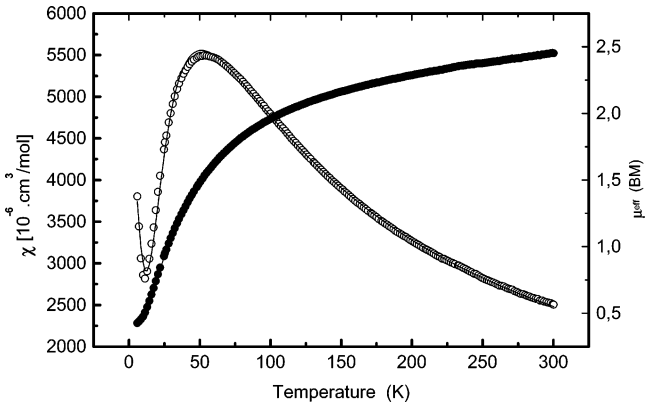

Figure 6. Magnetic susceptibility (χ, left scale) and effective magnetic moment (μ_{eff}, right scale) for complex **4**.

Magnetic Measurements. The temperature dependence of the magnetic susceptibility and the effective magnetic moment (μ_{eff}) of complex **4** are presented in Figure 6. The μ_{eff} value is 2.451 μ_B at 300 K and falls to 0.427 μ_B at 6 K, in agreement with an antiferromagnetic intramolecular coupling (singlet ground state). The susceptibility curve analysis was obtained using the isotropic spin−spin interaction by the Heisenberg−Dirac−Van Vleck Hamiltonian ($H = -JS_1 \cdot S_2$), where $S_1 = S_2 = {}^1/_2$, which is known as the Bleaney−Bowers[42] equation:

(41) (a) Orton, J. W. *Electron Paramagnetic Resonance*; London Life Books LTD: London, 1968. (b) Felthouse, T. M.; Laskowski, E. D.; Hendrickson, D. N. *Inorg. Chem.* **1977**, *16*, 1077−1089. (c) Bencini, A.; Gatteschi, D. *EPR of Exchange Coupled Systems;* Springer: New York, 1990.

(42) O'Connor. Magnetochemistry−Advances in Theory and Experimentation. In *Progress in Inorganic Chemistry*; Lippard, S. J., Ed.; 1982; Vol. 29, pp 203−283.

$$\chi = (1 - x_p)\frac{N_A g^2 \beta^2}{k(T - \Theta)}\left[\frac{\exp(2J/kT)}{1 + 3\exp(2J/kT)}\right] + 2\chi_p\frac{N_A g^2 \beta^2 S(S+1)}{3K(T - \Theta_J)} + 2(\mathrm{TIP}) \quad (1)$$

with

$$x = \frac{J}{kT}$$

and where x_p = paramagnetic fraction per monomer, N_A = Avogadro's number, g = isotropic splitting factor, β = Bohr magneton (0.927×10^{-2} erg/Oe), k = Boltzmann's constant, Θ = Weiss temperature per cluster (dinuclear), Θ_J = Weiss temperature for paramagnetic impurities, and TIP = temperature independent paramagnetism per monomer (per metal center). The best-fit parameters found were $J = -20.2 \pm 0.2$ cm^{-1}, $g = 2.18 \pm 0.1$, TIP $= 60 \times 10^{-6}$ cm^3/mol, $x_p = 5.0 \pm 0.2\%$, $\Theta = -68 \pm 0.1$ K, $\Theta_J = -6.0 \pm 0.5$ K, and $R = 1.189$.

The same analysis for complex **3** (Figure S3, Supporting Information) shows that the μ_{eff} value falls from $3.04\mu_B$ at 300 K to $1.06\mu_B$ at 2 K indicating a low antiferromagnetic intramolecular coupling. A $J = -13 \pm 2$ cm^{-1} parameter was fitted for complex **3**.

The $J = -13 \pm 2$ cm^{-1} and $J = -20.2 \pm 0.2$ cm^{-1} values fitted for complexes **3** and **4**, respectively, are lower than, but comparable with, that reported for the [([9]aneN3)Cu(μ-OH)$_2$Cu([9]aneN$_3$)]$^{2+}$ ($J = -45$ cm^{-1}) complex[43] in which a di-μ-hydroxo bridge was determined by X-ray crystallography. However, in the absence of crystal structures, one can only speculate as to the reason for a weaker antiferromagnetic coupling in complexes **3** and **4** compared to [([9]aneN3)Cu(μ-OH)$_2$Cu([9]aneN$_3$)]$^{2+}$.[43] In [([9]aneN3)Cu(μ-OH)$_2$Cu([9]aneN$_3$)]$^{2+}$ the tridentate 1,4,7-triazacyclononane ligand is facially coordinated and occupies two basal and the apical positions of the copper centers in a square-pyramidal arrangement. So, the Cu−(μ-OH)−Cu bonds are localized in the basal plane, and the (Cu(1)$d_{x^2-y^2}$)−O−(Cu(2)$d_{x^2-y^2}$) pathway contributes significantly to J. On the other hand, in the dinuclear complexes **3** and **4** one of the Cu−(μ-OH)−Cu bonds is most probably localized in the apical position (it is reasonable to assume a square-pyramidal arrangement around the copper centers in **3** and **4** from the meridional coordination form of the tridentate ligands in the mononuclear complexes **1** and **2**) which would yield weaker antiferromagnetic coupling through the (Cu(1)d_{z^2})−O−(Cu(2)d_{z^2}) pathway. From this information and from the EPR data, it is reasonable to assume that complexes **3** and **4** have dinuclear structures in which the Cu^{II} centers are bridged by a di-μ-hydroxo core as proposed in Chart 1. Furthermore, the physicochemical properties (EPR, CV) of **3** and **4** are also very similar and consistent with a Cu^{II}−(μ-OH)$_2$−Cu^{II} structure.

Reactivity of 1 and 2 toward Phosphodiester. The phosphodiester activity of the mononuclear Cu^{II} complexes **1** and **2** was investigated through the hydrolysis of the activated phosphodiester 2,4-BDNPP. In light of the formation of the mononuclear protonated/deprotonated species [LCu(OH$_2$)$_2$·LCu(OH$_2$)(OH) + H$^+$] and the equilibrium of the mononuclear/dinuclear species, the 2,4-BDNPP hydrolysis promoted by the copper(II) system is expected to be strongly dependent on the concentration of **1** and **2** and pH. As shown in Figure 7 and Figure S4 (Supporting Information), for both complexes, the pseudo-first-order rate constant (complex in excess) (k_{obs}) vs pH plots show sigmoidal curves, which were fitted by the Boltzmann model, and the following pK_a values were obtained: complex **1**, 8.78 ± 0.05, and complex **2**, 9.38 ± 0.02. These values are in good agreement with the dissociation constants of the complexes determined by potentiometric titration. These data strongly suggest that in both cases the catalyst is the [CuL(OH$_2$)(OH)]$^+$ species. The OH$^-$ ligand is therefore considered to be a good nucleophile for phosphodiesters.

The order of the reaction with respect to complexes **1** and **2** was investigated at their respective saturation pH values, and the rate constant (k_{obs}) vs complex concentration plots are presented in Figure 8 and Figure S5 (Supporting Information). As can be seen, both systems show a nonlinear

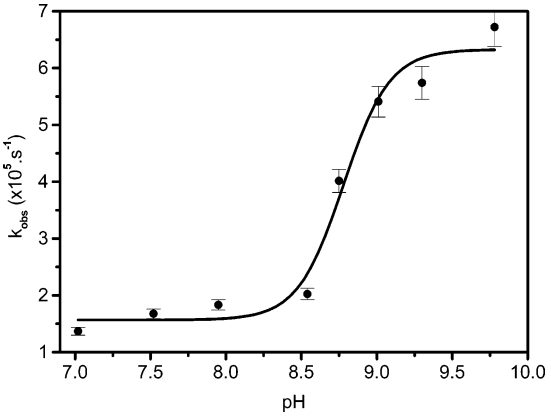

Figure 7. Dependence of the reaction rate on pH for the hydrolysis of 2,4-BDNPP promoted by complex **1**. Conditions: [2,4-BDNPP] = 5.0×10^{-5} mol L^{-1}; [complex] = 1.5×10^{-3} mol L^{-1}; buffer TRIZMA (pH 7.0−8.5) and CHES (pH 9.0−9.8); $I = 0.1$ mol L^{-1} (LiClO$_4$·3H$_2$O); $T = 50$ °C, in aqueous solution.

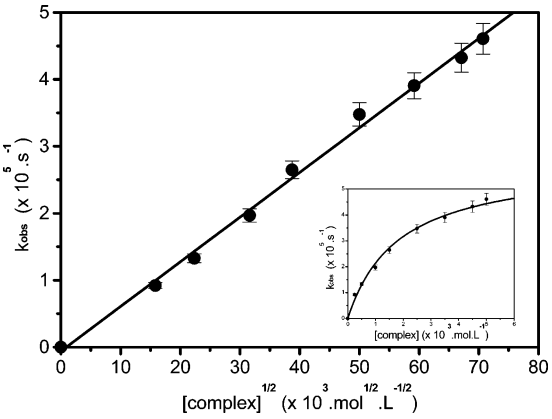

Figure 8. Dependence of the reaction rate on the complex **1** concentration for the hydrolysis of 2,4-BDNPP. Conditions: [2,4-BDNPP] = 5.0×10^{-5} mol L^{-1}; [complex] = 2.5×10^{-4} to 5.0×10^{-3} mol L^{-1}; buffer CHES (pH 9.3); $I = 0.1$ mol L^{-1} (LiClO$_4$·3H$_2$O); $T = 50$ °C, in aqueous solution.

(43) Chaudhuri, P.; Ventur, D.; Wieghardt, K.; Peters, E. M.; Peters, K.; Simon, A. *Angew. Chem., Int. Ed. Engl.* **1985**, *24*, 57−59.

Table 7. Kinetic Data for the 2,4-BDNPP Hydrolysis Promoted by Complexes **1** and **2** at 50 °C and an Excess of Complex **1** or **2**

complex	pK_a[a]	$k_{1/2}$ ($mol^{-1/2}$ $L^{1/2}$ s^{-1})[b]	K_f (mol^{-1} L)[c]	k (s^{-1})[d]
1	8.78 ± 0.05	(6.67 ± 0.17) × 10^{-4}	11.9 × 10^3	5.7 × 10^{-6}
2	9.38 ± 0.02	(3.07 ± 0.35) × 10^{-4}	12.8 × 10^3	4.3 × 10^{-6}

[a] Kinetic. [b] $R > 0.98$. [c] Valid only at the experimental pH since it is a pH dependent constant. [d] $k = K_2k_3$[substrate].

behavior and a saturation curve is attained. This observation has been reported for other Cu^{II} mononuclear complexes[8,14c,15b] and attributed to a dinuclear/mononuclear equilibrium, where the mononuclear $[Cu(L)(H_2O)(OH)]^+$ complex is the catalytically active species. This behavior has been[44] treated as a half-order dependence of the hydrolysis rate on the complex concentration, and so the initial rates vs $[complex]^{1/2}$ were plotted and linear fits were obtained (Figure 8 inset). From the linear fits the half-order constants were calculated, and they are shown in Table 7.

Burstyn and co-workers[15a] have deduced a half-order rate equation (eq 2) for such systems:

$$[LCu] = [(-0.5 + (2K_f[Cu_T])^{0.5}]/2K_f \qquad (2)$$

$$v = \frac{d[OR]}{dt} = k\left[\frac{(-0.5 + (2K_f[Cu_T])^{0.5}}{2K_f}\right]$$

where $k = K_2k_3[^-OPO(OR)(OR)]$, [LCu] = reactive mononuclear concentration, Cu_T = total copper concentration, and K_f = dinuclear−mononuclear equilibrium constant. Through this equation the dinuclear formation (K_f) and the first-order constants can be determined. Table 7 shows the values for complexes **1** and **2**. Due to the relatively high values for K_f we were able to isolate the dinuclear complexes **3** and **4**.

The dependence of the reaction rate on the substrate concentration was also investigated, and the experiments were carried out at the respective saturation pH of each complex. The initial rate (v_0) vs the [2,4-BDNPP] plots for complexes **1** and **2** are shown in Figure 9 and Figure S6 (Supporting Information), respectively. As can be observed for both complexes, initially, the cleavage rate increases linearly with the increase in [2,4-BDNPP], but deviates gradually from linearity and tends toward a saturation curve. In view of this behavior, the Michaelis−Menten model was employed and the data were fitted by the Lineweaver−Burk linearization method. The double reciprocal plots (1/[2,4-BDNPP] vs $1/v_0$) and the kinetic data are presented in the inset of Figure 9 and Table 8, respectively. When a 100-fold excess of substrate over the mononuclear complexes ([complex] = 1 × 10^{-6} M) was used, 18 and 7 turnovers were detected during 48 h, for **1** and **2**, respectively.

The fact that the complexes **1** and **2** follow the same rate law in the hydrolysis reaction of 2,4-BDNPP is evidence for identical mechanisms. Given that complexes **1** and **2** have similar structures, with the Cu^{2+} ions being in square-pyramidal coordination arrangements, which factors must be

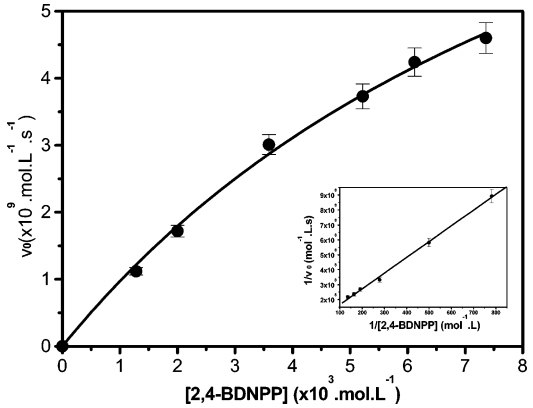

Figure 9. Dependence of the reaction rate on the 2,4-BDNPP concentrations for the hydrolysis reaction promoted by complex **1**. Conditions: [2,4-BDNPP] = 1.3 × 10^{-3} to 7.4 × 10^{-3} mol L^{-1}; [complex] = 5.0 × 10^{-5} mol L^{-1}; buffer CHES (pH 9.3); I = 0.1 mol L^{-1} ($LiClO_4 \cdot 3H_2O$); T = 50 °C, in aqueous solution.

Table 8. Kinetic Data for the 2,4-BDNPP Hydrolysis Promoted by Complexes **1** and **2** at 50 °C and an Excess of Substrate

complex	v_{max} (mol L^{-1} s^{-1})	K_M (mol L^{-1})	k_{cat} (s^{-1})	$K_{ass.}$ (mol^{-1} L)[a]	rate[b]
1	16.4 × 10^{-9}	17.3 × 10^{-3}	3.28 × 10^{-4}	57.8	121
2	7.02 × 10^{-9}	3.03 × 10^{-3}	1.40 × 10^{-4}	330.0	51.9

[a] $K_{ass.} = 1/K_M$. [b] Rate = k_{cat}/k_e, where k_e = 2.7 × 10^{-6} s^{-1} at 50 °C (noncatalyzed hydrolysis).[23,45]

responsible for the differences in the rate of hydrolysis of 2,4-BDNPP? The catalytic rate constant of 3.28 × 10^{-4} s^{-1} for **1** is more than twice the rate of **2** (1.40 × 10^{-4} s^{-1}) under the same experimental conditions. According to Burstyn et al.,[8,15] several factors, including (i) the monomer−dimer equilibrium, (ii) the bond angle between the two labile cis-oriented sites X−Cu−X, (iii) the Lewis acidity of the metal complex, and (iv) the equilibrium constant for the formation of the catalyst−substrate complex, should be taken into account.

From Table 8, one can see that the mononuclear−dinuclear equilibrium constants K_f are identical (∼12 × 10^3 M^{-1}) for the two complexes, and therefore similar concentrations of the active mononuclear catalysts $[LCu(OH_2)(OH)]^+$ must be present in the reactions. The X-ray crystal structures of **1** and **2** reveal that the Cl−Cu−Cl angles (102.49(4)° for **1** and 100.23(4)° for **2**) differ only slightly and should not contribute significantly to the differences observed in k_{cat}. Recently, by investigating the reactions of a series of related macrocycle copper complexes, it has been demonstrated that a difference of 4.0° in this angle does not affect the rate of hydrolysis of diester phosphates.[15c] In fact, if the compression of the cis angle were a determining factor in the present case, one would expect complex **2** to be more reactive (higher k_{cat}) than complex **1**.[15c] Therefore, other factors (iii and iv) are considered to influence the rate of hydrolysis here.

From the UV−vis spectral data in Table 5 it is reasonable to assume that the tridentate imine ligand HISMIMI is a poorer electron donor compared to the corresponding amine HISMIMA ligand, since the d−d absorption maximum for the $[Cu(HISMIMI)Cl_2]$ complex shifts to longer wavelengths consistent with a smaller d−d splitting. Consequently,

(44) Wilkins, R. G. *Kinetics and Mechanism of Reactions of Transition Metal Complexes*; VCH: Weinheim, 1991; pp 1−64.

Scheme 1. Proposed Mechanism for the 2,4-BDNPP Hydrolysis Promoted by **2**

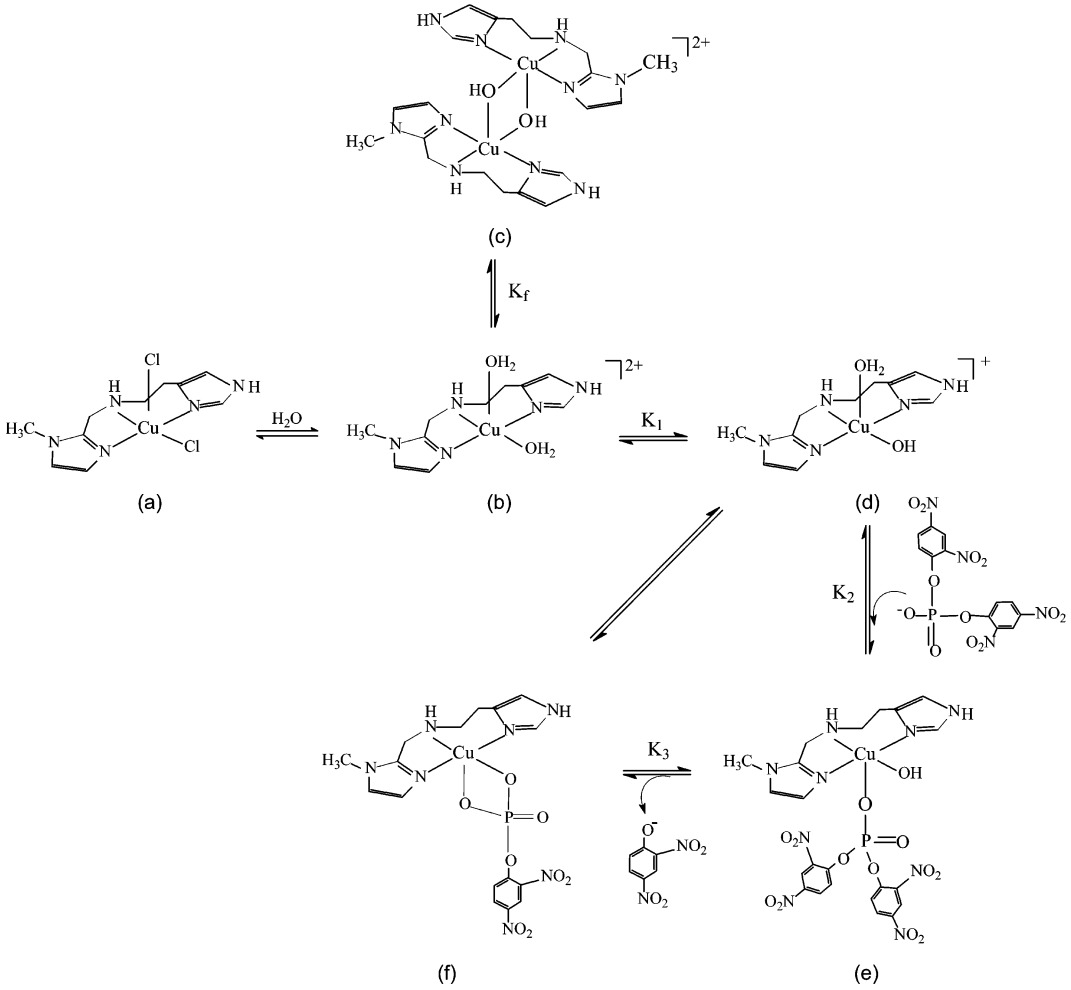

[Cu(HISMIMI)Cl_2] must be a stronger Lewis acid than [Cu(HISMIMA)Cl_2], and, as expected, the former complex shows the higher activity in the phosphodiester hydrolysis through intramolecular nucleophilic Cu^{II}−OH attack as revealed by the larger catalytic constant (k_{cat}) value. Interestingly, there is also a direct correlation between the Lewis acidity of complexes **1** and **2** and the apparent potentiometric/kinetic p*K*a values of their corresponding diaqua [LCu-(OH_2)]$^{2+}$ species (8.9 for **1** and 9.3 for **2**), indicating that in the present case Lewis acidity of the Cu^{II} centers significantly affects the rate of phosphate diester hydrolysis.

The kinetic data from Table 8 also reveal that the equilibrium constant $K_{ass.} \cong 1/K_M$ for the formation of the catalyst−substrate complex is significantly larger for the complex containing the secondary amine ligand. In fact, the opposite should be expected, because the [Cu(HISMIMI)-Cl_2] complex which contains the Schiff base is a stronger Lewis acid relative to [Cu(HISMIMA)Cl_2] and therefore should have a larger $K_{ass.}$. A plausible explanation for this observation may be related to the greater flexibility of the tridentate amine ligand compared to the more rigid imine ligand. Because copper complexes can easily deform, the HISMIMA amine ligand may allow a more favorable grouping of the coordinating atoms (ligand + phosphate diester) around the Cu^{II} ion than the Schiff base HISMIMI ligand which is constrained by conjugation effects to a planar configuration. Finally, complex **1** catalyzes the hydrolysis of 2,4-BDNPP with a 121-fold increase in the rate compared to the non-catalyzed reaction at 50 °C ($k_e = 2.7 \times 10^{-6}$ s^{-1}).[45]

In view of the X-ray structures and the kinetic behavior of complexes **1** and **2** in the hydrolysis of 2,4-BDNPP, we suggest a mechanism which is similar to that proposed for [Cu[9]aneCl_2]. In Scheme 1 we show the proposed mechanism using complex **1** as the catalyst, and the following experimental results corroborate this proposal: (i) complex **1** (a) was structurally characterized and contains a *cis*-$CuCl_2$ moiety; (ii) species (b) can be suggested, taking into account the lability of the Cu−Cl bonds of **1** in aqueous solution—conductivity measurements and potentiometric titrations are in line with this proposal; (iii) complex (c) was isolated and characterized as a Cu(μ-$OH)_2$Cu species (magnetic susceptibility measurements) and evidenced in solution by CV and EPR; (iv) the presence of species (d) as the active catalyst is supported from potentiometic titration and the dependence of k_{obs} on the pH of the solution. All attempts to isolate the product (f) containing the monoester under the kinetic experimental conditions were unsuccessful even when using unactivated phosphodiesters such as diphenylphosphate. When stoichiometric reactions between 2,4-BDNPP and complexes **2** and **4** in CH_3OH were carried out for long

(45) Kirby, A. J.; Younas, M. *J. Chem. Soc. B* **1970**, 510−513.

periods, the starting complexes were isolated. Taking these experimental results together we suggest that the bonded phosphate monoester in the product (f) must be displaced by solvent molecules completing the catalytic cycle. It is important to note that the catalyst is the $Cu(OH_2)(OH)$ species (d), as evidenced by the pH dependence on the velocity of the reaction, in which the nucleophile OH^- is coordinated in the equatorial position. Thus, the interaction of the substrate most probably occurs by displacement of the axially coordinated water molecule (e) prior to the intramolecular attack of the nucleophile leading to the product (f) and 2,4-dinitrophenolate. This last point represents the main difference between the mechanism proposed here and that for the analogous[14c] $[Cu(BMPA)Cl_2]$ system, where an equatorial coordinated phosphate intermediate was proposed.

DNA Cleavage. Interaction of 1 with Calf Thymus DNA. Interaction of **1** with CT-DNA was investigated by cyclic voltammetry. Cyclic voltammograms of **1** in CHES buffer, at pH 9.3, 50 °C, and under argon are shown in Figure S7 (Supporting Information). As can be observed, the presence of DNA in the solution at the same concentration of **1** caused a significant change in the CV. With respect to the reduction potential, addition of CT-DNA results in a cathodic shift of E_{pc} from −434 mV (vs Ag/AgCl) at $R = 0$ to −531 mV at $R = 2.5$, where $R =$ [CT-DNA]/[**1**]. This result is in agreement with the hypothesis of interaction between **1** and DNA involving the copper (II) ion, since a shift in the cathodic peak which is assigned to the $Cu^{II} \rightarrow Cu^{I}$ process indicates that reduction of the copper center becomes more difficult when DNA is added. This, in turn, can be explained in terms of an increase in electronic density around the Cu^{II} ion due to the presence of a long polyanionic phosphate chain interacting electrostatically with the metal center. In addition to the change in the reduction potential, the voltammetric current also decreases significantly upon addition of DNA. Its initial value in the absence of DNA is 3.68 μA and addition of DNA results in a current of 2.21 μA when the ratio between CT-DNA and complex **1** is 2.5. This behavior is also consistent with the hypothesis of interaction between **1** and CT-DNA, since such association results in higher size adduct with lower diffusion coefficient, when compared to that of the free complex.

Cleavage of Double-Stranded DNA by 1. Complex **1** is able to cleave genomic DNA (gDNA, linear double stranded DNA extracted from mussels), after 24 h incubation at 50 °C. At the higher metal concentration gDNA is more than 95% degraded (Figure S8, Supporting Information).

To further analyze the reaction mechanism, pUC18 plasmid DNA cleavage was tested at different pH values (pH 7.0, 7.5, 8.0, and 8.5, 0.2 M Tris-HCl; and pH 9.3, 0.2 M CHES; Figure S9, Supporting Information), according to potentiometric titrations indicating the presence of the H_2O and/or hydroxo species. Incubation at higher pH (9.3) promoted a greater amount of degradation (47.2%) than at lower pH values (24.6% at pH = 8.0), thus establishing a relationship between the presence of the hydroxo species and the extent of cleavage reaction. Moreover, at pH = 9.3,

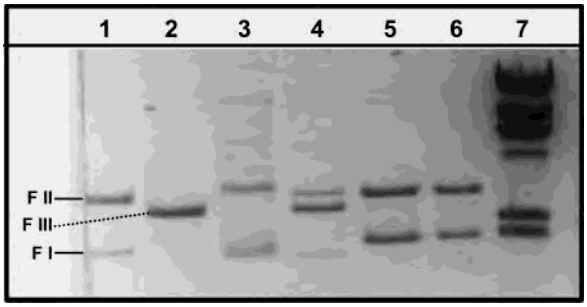

Figure 10. T4 ligase treatment of complex **1** cleaved plasmid DNA. Lane 1: control pUC18 plasmid DNA. Lane 2: *Eco*RI digested pUC18. Lane 3: T4 ligase treatment of *Eco*RI digested pUC18. Lane 4: T4 ligase treatment, in the presence of complex **1** (0.4 mM), of a previously *Eco*RI digested pUC18. Lane 5: T4 ligase treatment of complex **1** treated pUC18. Lane 6: complex **1** treated pUC18 purified by ethanol precipitation before T4 ligase treatment. Lane 7: λ DNA *Hin*dIII digest. All incubations were performed at pH 8.0; 50 °C for 24 h.

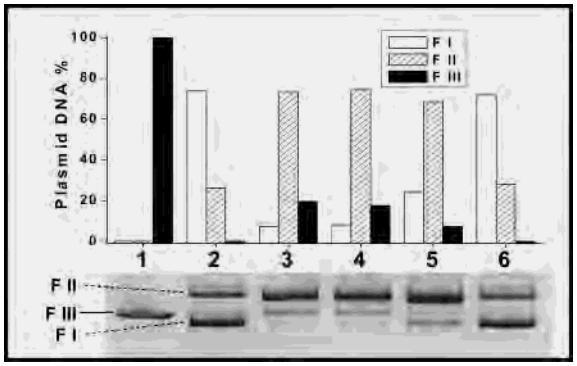

Figure 11. Hydroxyl radical scavengers did not inhibit cleavage by complex **1**. Lane 1: *Bam*HI digested pBSK-II. Lane 2: control plasmid DNA. Lane 3: plasmid DNA, 3.75 mM complex **1**. Lane 4: plasmid DNA, 3.75 mM complex **1**, 0.4 M DMSO. Lane 5: plasmid DNA, 0.1 mM $Fe(EDTA)^{2-}$, 10 mM DTT. Lane 6: plasmid DNA, 0.1 mM $Fe(EDTA)^{2-}$, 10 mM DTT, 0.4 M DMSO. All samples were incubated in 100 mM CHES buffer pH 9.30, for 24 h at 50 °C. Above the image of the gel is shown a histogram of the quantified plasmid DNA forms observed in the gel.

complex **1** is able to degrade the relaxed circular form II to the linear form III (lane 1 at pH = 9.3 of Figure S9). T4 ligase was ineffective in promoting the religation of DNA fragments previously cleaved by complex **1**. Complex **1** interferes with T4 ligase activity as shown in Figure 10, lane 4. For this reason complex **1** treated DNA was purified by ethanol precipitation to eliminate excess complex **1** from the reaction medium. However, even after DNA purification, cleaved DNA could not be religated (Figure 10, lane 6). We thus propose that either products of DNA cleaved by complex **1** may not be 3′-OH and 5′-PO_4 or complex **1** remained bound to the DNA after cleavage; in these two situations T4 ligase would be unable to religate DNA fragments. The hydroxyl radical scavengers glycerol (Figure S10, Supporting Information) or dimethyl sulfoxide (Figure 11, lanes 3 and 4) did not interfere with the DNA cleavage activity of complex **1**, thus suggesting that diffusible hydroxyl radicals were not involved in the cleavage reaction. A parallel experiment by using the oxidative cleaving system $[Fe(EDTA)]^{2-}$/DTT in the absence (lane 5) and in the presence of 0.4 M DMSO (lane 6) demonstrated the efficiency of DMSO as a radical scavenger. In addition, the presence of 0.12 μM cerium sulfate in the cleavage reaction (not shown)

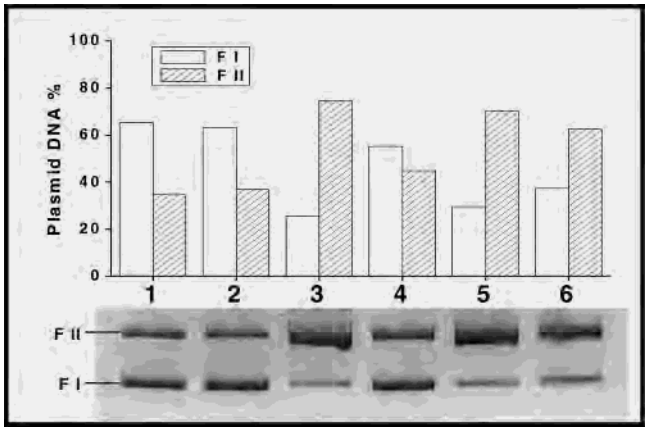

Figure 12. Anaerobic × aerobic plasmid DNA cleavage. Lanes 1−3: anaerobic conditions. Lanes 4−6: aerobic conditions. Lanes 1 and 4: control plasmid DNA. Lanes 2 and 5: plasmid DNA, 0.1 mM $Fe(EDTA)^{2-}$, 10 mM DTT. Lanes 3 and 6: plasmid DNA, 3.75 mM complex **1**. All samples were incubated in 100 mM CHES buffer pH 9.30 for 4 h at 50 °C. Above the image of the gel is shown a histogram of the quantified plasmid DNA forms observed in the gel.

of **1** guaranteed the presence of Cu^{II} and had no effect on the cleavage of the double stranded plasmid DNA, which suggest that an oxidative mechanism for this reaction is unlikely. To definitively confirm this hypothesis and to probe the possible participation of molecular oxygen in the cleavage of DNA by **1**, reactions were also performed under rigorously anaerobic conditions (Figure 12). The possibility of the presence of residual oxygen under anaerobic conditions was completely discarded by carrying out parallel experiments with the $[Fe(EDTA)]^{2-}$/DTT system (Figure 12, lane 2).[15a] Under these conditions, no DNA degradation was observed over a period of 4 h, at pH = 9.3 and 50 °C (compare lanes 1 and 2). As can be seen by comparing lanes 3 and 6, complex **1** effectively cleaves double stranded DNA even in the absence of oxygen to approximately the same extend as that observed in the experiment under aerobic conditions. Thus, we conclude that the cleavage of DNA by **1** in anaerobic experiments is oxygen independent and that this reaction most probably occurs through a hydrolytic mechanism as proposed in the reaction of **1** with the model 2,4-BDNPP substrate.

Complex **1** activity toward plasmid DNA was carefully followed over a time period of 24 h, with [**1**] = 2 mM at 50 °C. A pseudo-first-order rate constant of 0.28 h^{-1} and a half-life of 2.4 h were obtained by analysis of the data given in Figure 13. A comparison of this rate constant with values reported in the literature reveals that complex **1** is about five times more effective than the Cu^{II}−triamine complexes reported by Burstyn and co-workers (0.04−0.09 h^{-1} at 50 °C), but the efficiency is similar to that of lanthanoid

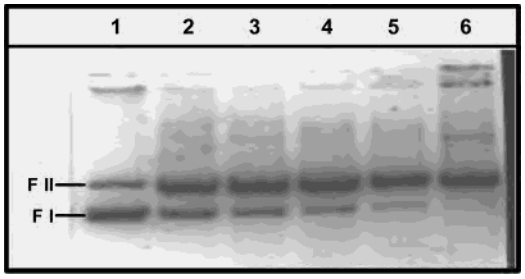

Figure 13. Kinetic analysis of complex **1** DNA cleavage activity. Plasmid DNA (pBSKII, 4 mM phosphodiester links) and 2 mM complex **1** were incubated at pH 9.3 (200 mM CHES), 50 °C for 0, 2, 4, 6, 8, or 24 h (lanes 1−6, respectively).

cations and their complexes (e.g., $[Eu^{3+}]$ = 2.5 mM with k = 0.25 h^{-1} at catalyst concentration used for Michaelis−Menten analysis). Higher efficiencies have been reported for a Co^{III}−polyamine system with k = 0.82 h^{-1} at [catalyst] = 1 mM and for a Cu^{II}−1,3,5-triaminocyclohexane system (k = 4.3 h^{-1}), all determined under identical experimental conditions.

Conclusion

In summary, we have synthesized and structurally characterized two new mononuclear *cis*-dichloro Cu^{II} complexes containing biologically relevant N-donor ligands. In aqueous solution these complexes generate the *cis*-aqua/hydroxy species which catalyze the hydrolysis of the phosphodiester 2,4-BDNPP substrate with ∼100-fold enhancement in the reaction rate in comparison to the spontaneous hydrolysis. Finally and most importantly, we have demonstrated that the $[Cu(HISMIMI)(OH_2)(OH)]^{1+}$ complex is capable of promoting the cleavage of plasmid DNA in a pH dependent reaction, even in the absence of molecular dioxygen, most probably through a hydrolytic mechanism with a rate constant of 0.28 h^{-1}, in accordance with the mechanism proposed for 2,4-BDNPP hydrolysis.

Acknowledgment. This work was supported by grants from CNPq, CAPES, PRONEX, CTPETRO, International Foundation for Science (A/2846), and Third World Academy of sciences (RG-BIO-LA 099). W.A.O. and W.A.C.P. gratefully acknowledge financial support from FAPESP.

Supporting Information Available: X-ray crystallographic details for complexes **1** and **2** in CIF format. Figure S1 (species distribution for **2**); Figure S2 (CV for **1**); Figure S3 (magnetochemistry for **3**); Figures S4, S5, and S6 (kinetic details for **2**); Figure S7 (CV of **1** in the presence of CT-DNA); Figure S8 (genomic DNA cleavage by **1**); Figures S9 and S10 (plasmid DNA cleavage by **1**). This material is available free of charge via the Internet at http://pubs.acs.org.

IC026277C